Rapid communication

Journal of RAMAN SPECTROSCOPY

Received: 15 October 2016 Revised: 9 January 2017 Accepted: 10 January 2017 Published online in Wiley Online Library: 10 February 2017

(wileyonlinelibrary.com) DOI 10.1002/jrs.5112

In-situ Raman study of phengite compressed in water medium under simultaneously high *P–T* parameters

S. V. Goryainov,[a]* A. S. Krylov,[b] O. P. Polyansky[a] and A. N. Vtyurin[b]

The *in-situ* method of Raman spectroscopy was used to study the layered mineral phengite, $K(Al,Mg)_2(Si,Al)_4O_{10}(OH)_2$, compressed in water under simultaneously high temperatures and pressures (respectively, up to 373 °C and 12.5 GPa). The implemented conditions were typical of modeling the 'cold' subduction zones in lithospheric slabs. The high pressures and temperatures were produced in an electrically heated diamond-anvil cell. Measured Raman spectra have demonstrated a high *P–T* stability of the mineral. No non-quenchable phengite states (no reversible or irreversible polymorphic transitions, overhydration or notable amorphization) were observed in the investigated samples. Copyright © 2017 John Wiley & Sons, Ltd.

Keywords: Raman spectra; phengite; high pressure; high temperature; diamond anvil cell

Introduction

Investigation of the interaction of silicates with water under subduction *P–T* conditions provides a better insight into the general geobalance and transportation of water and other volatile components in the subduction zones of lithospheric slabs.[1,2] The presence of large amounts of rock in the submerging oceanic crust makes possible water transportation to large depths. In addition to the major water transporters (serpentines), participation of other high-baric minerals, phengite,[3,4] datolite,[5] pyrophyllite[6] and talc,[6–8] was analyzed. Among those minerals, phengite remains a less studied material.

Phengite, $K(Al,Mg)_2(Si,Al)_4O_{10}(OH)_2$, is a potassic dioctahedral mica. The crystallographic structure of this mineral is close to that of muscovite, yet phengite has a higher content of Mg cations.[9] According to the International Mineralogical Association nomenclature,[4] phengite is a solid solution with general chemical formula $K(Al,Mg)_2(Si,Al)_4O_{10}(OH)_2$ whose extreme members are given by the following dioctahedral mica minerals: muscovite $KAl_3Si_3O_{10}(OH)_2$, aluminoceladonite $KAlMgSi_4O_{10}(OH)_2$ and celadonite $KMgFe^{3+}Si_4O_{10}(OH)_2$. In phengite minerals ultrahigh-baric complexes, the Si content exceeds that of rocks taken from shallower depths.[4,10,11] The latter correlation was laid to the basis of the geothermobarometer model of ultrahigh-baric minerals.[11]

The *in-situ* states of micas at high pressures still remain a scantily studied matter. Comparable *in-situ* *P–T* X-ray diffraction study of muscovite and paragonite (Na-muscovite) was performed up to 5 GPa and 600 °C.[12] Note a recent IR-spectroscopy study of micas (muscovite, biotite and phlogopite) under high pressures up to 30 GPa, and a Raman study of muscovite under pressures up to 8 GPa.[13] The widths of IR absorption bands in mica samples compressed in KBr medium were found to show a weak growth observed as the pressure *P* was increased to ~16–17 GPa. Then, a nonlinear growth of the intensity of those bands began, which circumstance could be distinctly traced considering the pressure dependence of the bandwidth of the 3640-cm^{-1} O–H stretching band in muscovite.[13] At pressures above 18–20 GPa, growth of disorder in the muscovite structure related with the notable growth of disorder in the arrangement of OH hydroxyl groups was detected.

Phengite is assumed to be a medium in the transportation of water into slab subduction zones, this mineral being, due to its high *P–T* stability, among the most deeply lying hydrated water-transporting minerals.[1,14] Previously, *ex-situ* phase analysis of products was performed to examine dehydration melting of phengite at pressures 1.5–3 GPa and temperatures 800–950 °C.[14] Note also that, in an earlier papers,[3] *in-situ* baric (up to 7.4 GPa) dependences of phengite unit-cell parameters, exhibiting small deviations from the Birch–Murnaghan dependence (for parameters a/a_0 and b/b_0), were reported; however, no refined data for atomic coordinates in that $2M_1$ phengite at high pressures were examined. Structural evolution of $2M_1$ and $3T$ phengite specimens (full structural data) with pressure up to 11 GPa[15,16] was presented. The experiments were performed using a quasi-hydrostatic water–alcohol medium (methanol/ethanol/water 16:3:1). It was found that, under pressure, the K-polyhedra deformed most readily, the MO_6 octahedra, less readily, and the TO_4 tetrahedra retained their stiffness.[15] A strong decrease of crystallinity occurring at pressures $P > 15$–17 GPa and room temperature was reported.

A literature survey shows that phengite and its *P–T* diagram were only examined by performing an *ex-situ* analysis of phengite samples following the high-baric experiments; hence, the real state of

* *Correspondence to: Sergei V. Goryainov, Sobolev Institute of Geology and Mineralogy SB RAS, Academician Koptyug Avenue 3, Novosibirsk 630090, Russia. E-mail: svg@igm.nsc.ru*

a *Sobolev Institute of Geology and Mineralogy SB RAS, Academician Koptyug Avenue 3, Novosibirsk 630090, Russia*

b *Kirensky Institute of Physics SB RAS, Akademgorodok, Krasnoyarsk 660036, Russia*

the samples under high *P–T* parameters, including the structure and vibration properties of the mineral, has never been examined by *in-situ* structural and spectroscopic methods. Using *in-situ* techniques, one can observe transitions into non-quenchable states, including, for instance, reversible polymorphism, hydration-degree changes or amorphization. Because phengite has a layered structure,[9] a hypothesis was put forward that, at high pressures, incorporation of additional H_2O or OH^- groups into the interlayer space of the mineral was possible. This assumption was made considering the overhydration data for various framework aluminosilicates.[17–20]

The purpose of the present study was to reveal possible presence of non-quenchable states of phengite in the domain of existence of the mineral at *P–T* parameters that model the conditions in the 'cold' subduction zones of lithospheric slabs. For reaching this goal, we used *in-situ* Raman measurements performed at high pressures and temperatures. Such conditions were obtained in a resistively heated diamond-anvil cell (DAC).

Methods and samples

Raman spectra were excited by a Spectra-Physics Ar^+ laser at 514.5-nm wavelength and registered on a Horiba Jobin Yvon triple spectrometer (model T64000).[5] The radiation power incident onto the sample during measurements was 5 mW. The spectra were recorded in the region from 10 to 4000 cm^{-1} at 2-cm^{-1} resolution. The Raman study of the processes proceeding in phengite samples at high hydrostatic pressures and temperatures was carried out using a resistively heated DAC with Diacell μScopeDAC HT(G) membrane-type anvils purchased from EasyLab (UK).[7,21] The cell had a water-cooled casing. During measurements, the anvils were blown with an inert argon flow with a 1% admixture of H_2. In the experimental arrangement, an Inconel gasket, initially 250 μm thick, was used. The gasket, squeezed at its periphery to a thickness of 80 μm, had a 150-μm hole prepared using a spark discharge. The pressure was determined from photoluminescence data (R1 and R2 lines) taken from a ruby piece mounted in the working volume of the cell. Accuracy of *P* determination is equal to ±0.05 GPa. Calibration of temperature (dependence of the sample temperature on the thermocouple temperature; the last is determined with accuracy ±0.5 °C) was performed by method.[22,23] The accuracy of this method in the sample temperature (*T*) determination is estimated as ±5 °C. The maximum *P–T* values reached in our experiments with phengite specimens were 12.52 GPa and 373 °C. Our experimental *in-situ* runs for studying of phengite–water system at simultaneously high *P–T* parameters are shown in Fig. 1, compared with *P–T* phase diagram of water-saturated phengite–hollandite.[1,24–26]

Phengite specimens cut from garnet–omphacite eclogite rock of the low layer of Maksyutov ultra-high-pressure metamorphic complex (South Ural Mountains, Russia) were mineral samples selected from the IGM mineral collection (Novosibirsk). Chemical composition of our phengite specimens, $K_{0.86}Na_{0.03}$ $(Al_{1.38}$ $Mg_{0.37}$ $Fe_{0.25})$ $(Ti_{0.03}$ $Al_{0.51}Si_{3.46})O_{10}$ $(OH)_2$, was determined in the work.[27] Lattice-dynamical simulations of C 2/c monoclinic phengite were performed with LADY software packet successfully used for many crystals.[28–32]

Results

On variation of pressure *P*, we observed monotonic variations of Raman spectra of phengite measured in the vibration regions of

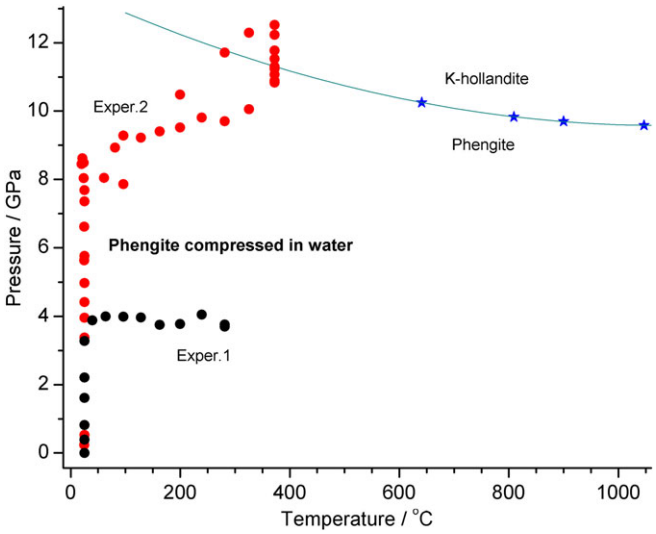

Figure 1. *P–T* phase diagram of water-saturated phengite–hollandite according to *ex-situ* data[1,24,25] and our experimental points of two *in-situ* runs for phengite–water system marked by black circles (experiment-1) and red circles (experiment-2). The theoretical estimations[24] are shown by stars, whereas the extrapolation of these data is plotted with blue–green curve.

octahedral–tetrahedral sheet and extra-sheet cations and, also, in the region of O–H stretching vibrations (Figs 2 and 3). With the increasing *P*, the 97, 191, 265, 423, 704 and 1095-cm^{-1} band wavenumbers v_i exhibited a monotonic shift toward higher values, whereas the O–H stretching band wavenumber showed a shift to lower values. The widths of all bands w_i are primary increased with *P–T* growth (see example for 704-cm^{-1} band in Figs 4 and 5). Note that the intensities of the major 265 and 704-cm^{-1} bands showed almost no changes, whereas the 191-cm^{-1} band decreased and the 423-cm^{-1} band increased in intensity with the increasing *P*.

The Raman spectrum of our phengite specimens exhibited three most intense Raman bands, two bands being observed in the wavenumber region below 1200 cm^{-1} and the third, 3612-cm^{-1}, band being a band due to the O–H stretching vibrations of hydroxyl groups. A simplest interpretation of the spectrum is as follows: the band at 265 cm^{-1} was due to the external vibrations of the TO_4 tetrahedra that formed the aluminosilicate layer and the band at 704 cm^{-1} was due to the O–T–O bending vibrations coupled with the M–O stretching vibrations of MO_6 octahedra. This interpretation is analogous to the one accepted for the vibration modes of other micas.[33–35]

To produce detailed interpretation of observed modes, the calculations of lattice dynamics of phengite were performed with LADY software packet using Born–Karman model.[31] Examples of calculated form of atomic vibrations for 265, 423 and 704-cm^{-1} bands are exhibited in Figs 6 and 7. Factor group vibration analysis of phengite crystal of monoclinic C 2/c symmetry leads to total numbers of optical modes $31A_g + 32B_g + 30A_u + 30B_u$ (at empty M1 site) and acoustical modes $A_u + 2B_u$. Observed and calculated Raman spectrum as well as its interpretation are shown in Table 1.

The presented interpretation of $2M_1$ phengite several modes is similar to that of $2M_1$ muscovite modes calculated in,[33] for instance, the strongest 704-cm^{-1} band (A_g 703-cm^{-1} band observed in muscovite) is due to the bending O–T–O and T–O–T vibrations, in which the O atoms exercise dominant displacements along the *z*-axis, those displacements being the off-plane ones with respect to the octahedral–tetrahedral layer, and M–O stretching vibrations:

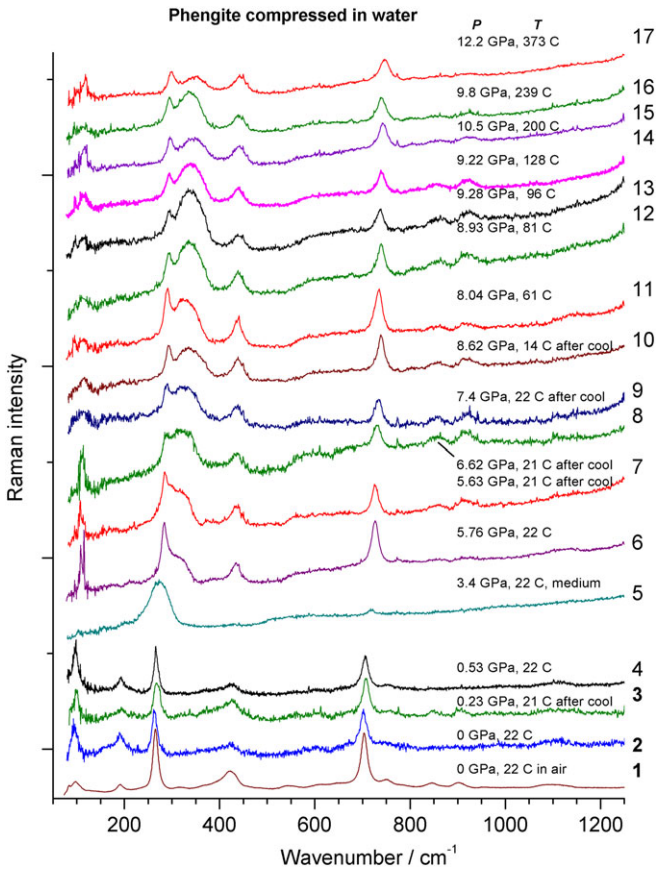

Figure 2. Raman spectra of phengite specimens compressed in water medium at indicated *P–T* conditions. The spectra were measured in the spectral region of 50–1250 cm^{-1}.

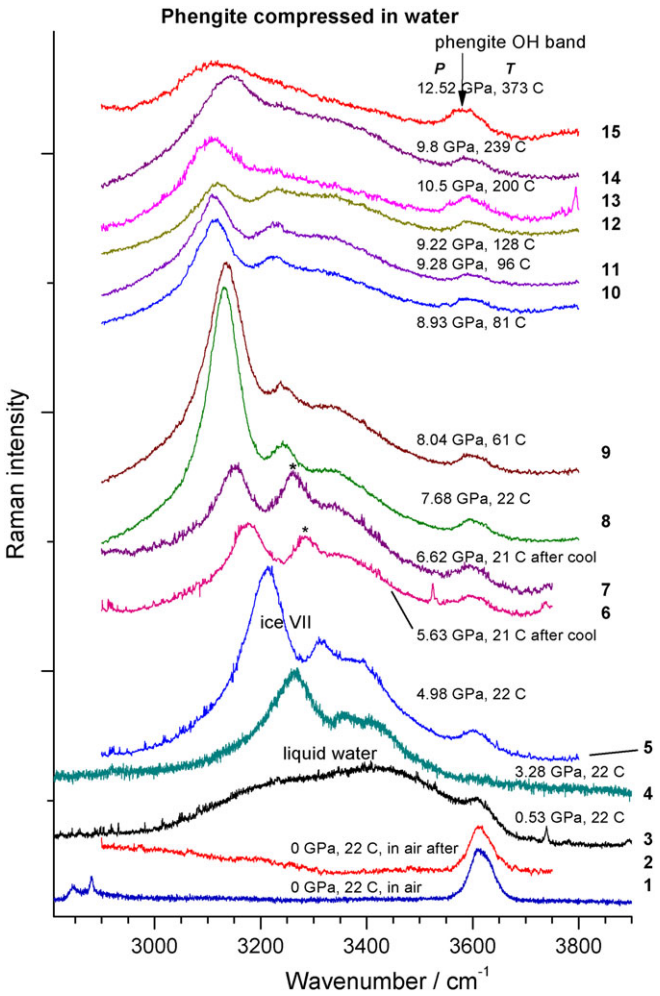

Figure 3. Raman spectra of phengite specimens compressed in water medium at indicated *P–T* conditions. The spectra were measured in the region of O–H stretching vibrations.

{(O3,O4,O5) breath$_z$ + O–T–O bend + T–O–T bend + M2–O2 stretch} in our interpretation (Table 1) and {O_{nb} z-trans + O_{br} z-trans + M2–O_b stretch} of muscovite in interpretation of McKeown *et al.*[33]

Our 704-cm^{-1} band is accidental doublet with very similar form of vibrations (v_{13} and v_{14} in Table 1). This can explain that 704-cm^{-1} doublet band width of 15.4 cm^{-1} (see Fig. 5) is greater than that of 265-cm^{-1} single band width of 12.7 cm^{-1} (both at 1 bar and 22 °C) and also the increase of this distinction with increasing *P–T* parameters to 12.5 GPa and 373 °C, at that widths reach the values of 24 and 14.8 cm^{-1}, respectively. The last is a result of slightly different slopes dv_i/dP and dv_i/dT for each component.

Our simulations supply a new point of view about very strong Raman modes of phengite at 704, 423 and 265 cm^{-1}, describing theirs as breathing modes changing the thickness of octahedral–tetrahedral layer with different participations of inner layered sublattices, moving along the *z*-direction. The 704-cm^{-1} doublet modes involve the movements of (O3,O4,O5) sublattices. The 423-cm^{-1} mode presents the movements of (O6,O3,O4,O5,T) sublattices, whereas the 265-cm^{-1} mode involves the movements of (O5,O2,O3,T) sublattices.

According to our simulations, low-wavenumber bands are attributed to external vibrations of tetrahedra: TO_4 trans + TO_4 rot, whereas modes of translational vibrations of K cations have very weak Raman intensity. Suddenly, the symmetric T–O stretching mode in phengite structure has very low calculated intensity and is not detected in Raman spectra. The v_{19} band at 1095 cm^{-1}

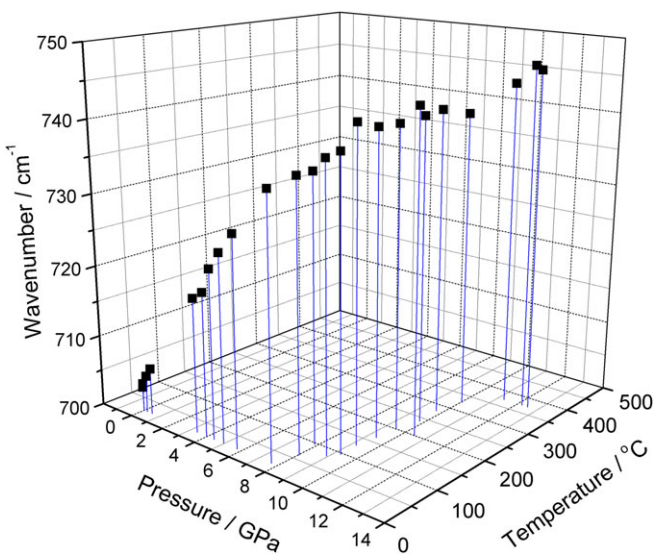

Figure 4. The wavenumber of the 704-cm^{-1} Raman band of phengite *versus* pressure *P* (in the range from 10^5 Pa to 12.5 GPa) and temperature *T* (in the range from 22 to 373 °C).

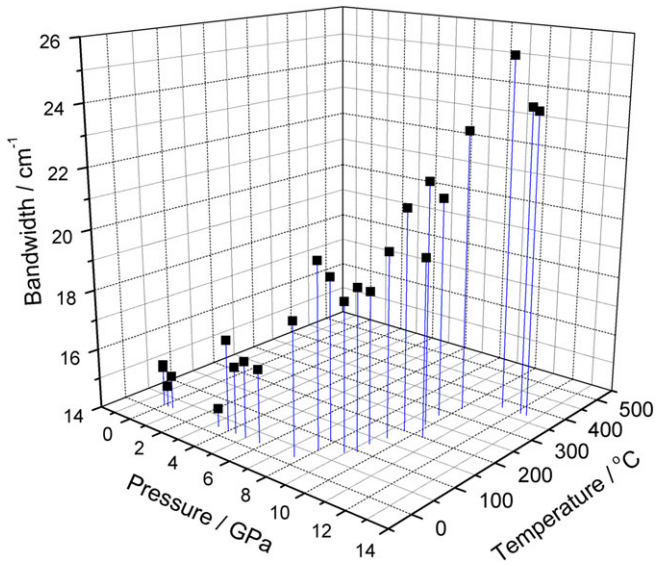

Figure 5. The width of the 704-cm^{-1} Raman band of phengite *versus* pressure *P* (in the range from 10^5 Pa to 12.5 GPa) and temperature *T* (in the range from 22 to 373 °C).

(Table 1) is interpreted as T–O stretching A_g mode having the small-medium intensity.

The bands at 265 and 704 cm^{-1} both exhibit high thermobaric stability, with their intensities and wavenumbers showing relatively small variations with the increase of *P*–*T* parameters, whereas the 423-cm^{-1} band shows the increasing intensity at growth of *P* (Fig. 2).

Also, the Raman spectra exhibit the bands due to the vibrations of liquid water medium and ices that appear and disappear with change of *P*–*T* (Figs 2 and 3). According to data,[36–38] cubic ice VII could transform to ice VII′ of lower symmetry, presumably tetragonal, at pressure about 10–14 GPa involving changes in the proton ordering/disordering that is enhanced at the heat. We could interpret the 14 spectrum in Fig. 3 as result of appearance of ice VII′ that differ from 8 to 13 spectra of ice VII. Raman O–H stretching spectrum of the medium changes at transition to liquid state (Fig. 3 (15)).

The strong band at 3612 cm^{-1} and its shoulder at 3624 cm^{-1} in the Raman spectrum of phengite are interpreted as A_g and B_g O–H stretching modes of the hydroxyl group, respectively (v_{21} and v_{22} in Table 1). There is also an additional weak C–H stretching bands at 2846 and 2882 cm^{-1}, observed in several spectra and interpreted as organic defects in the interlayer space (Fig. 3 (1)).

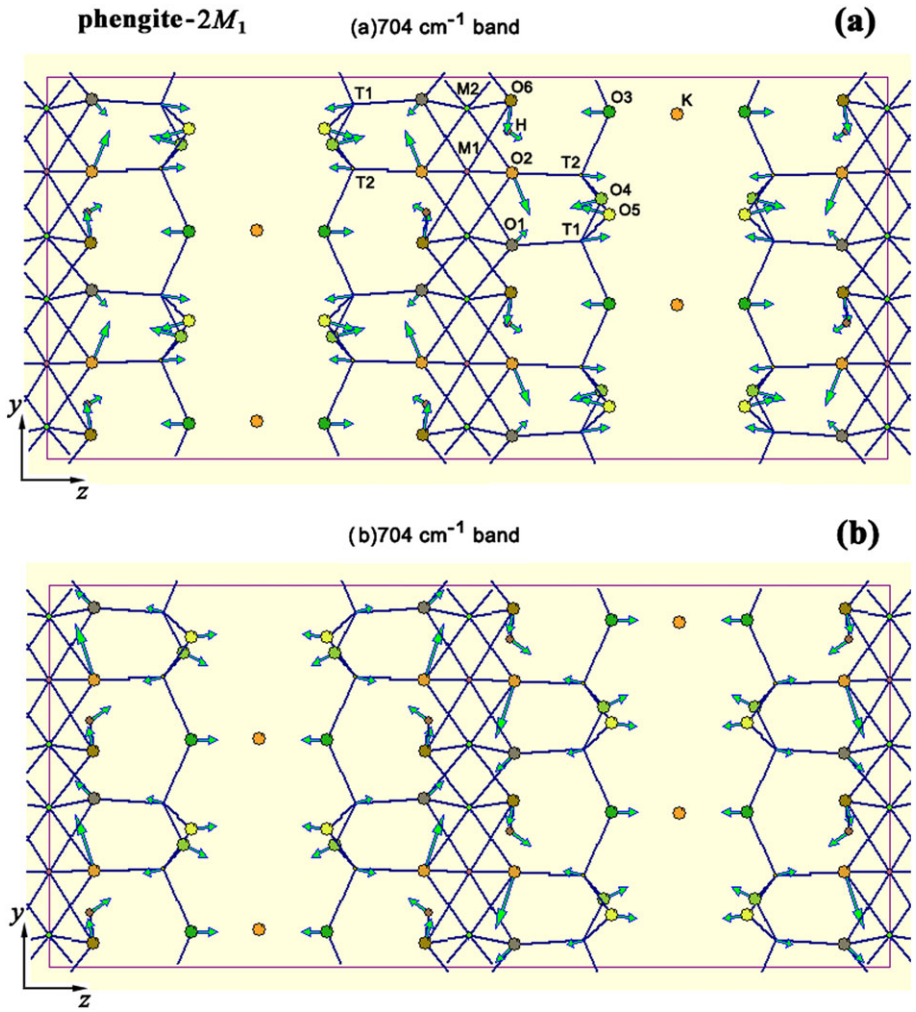

Figure 6. Calculated atomic motions for normal modes of phengite structure in *z*–*y* projection: (a) and (b) are components of the strongest (a) 704- and (b) 704-cm^{-1} doublet band, unresolved in Raman spectrum. Arrows show relative amplitudes of each atom.

Journal of RAMAN SPECTROSCOPY

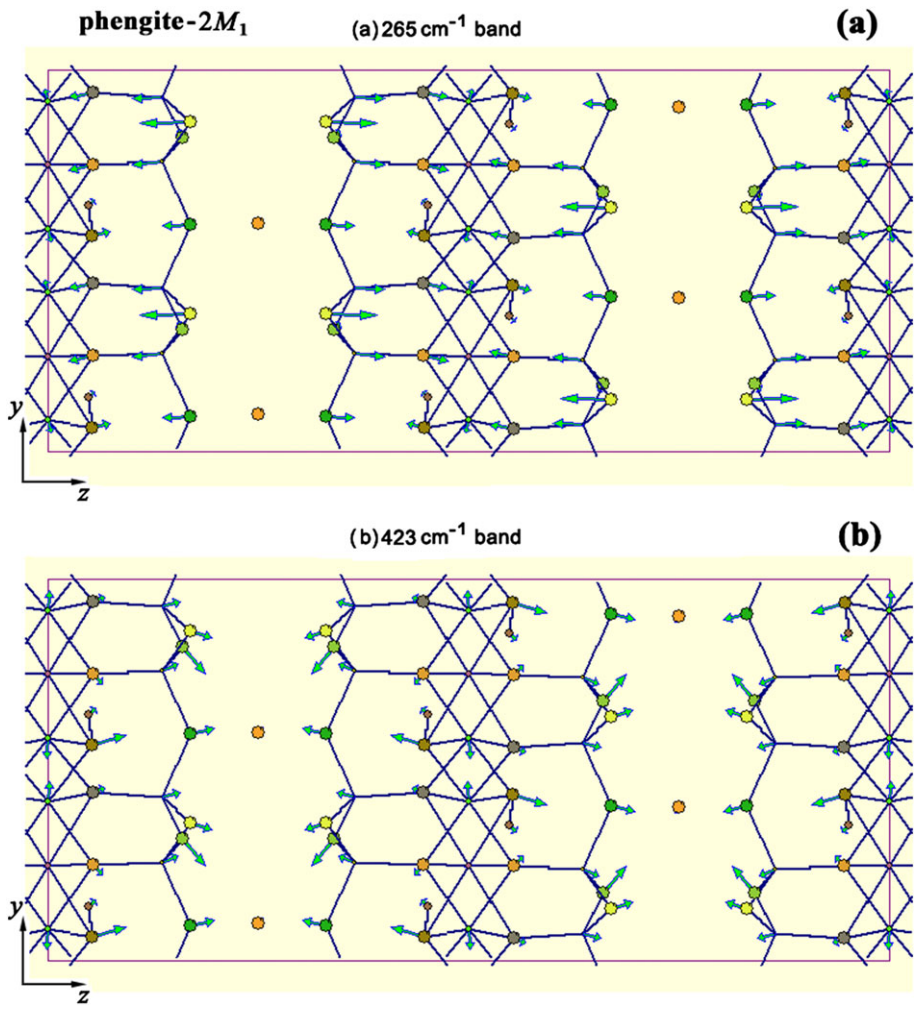

Figure 7. Calculated atomic motions for normal modes of phengite structure in *z*–*y* projection: 265-cm^{-1} (a) and 423-cm^{-1} bands (b) observed in Raman spectrum. Arrows show relative amplitudes of each atom.

Raman spectrum of cubic ice VII exhibits the strongest $v_1(A_{1g})$ O–H band and medium intensity satellite $v_3(E_g)$ and $v_3(B_{1g})$ O–H bands.[39] *In-situ* structural and Raman data of ice VII at simultaneously high *P*–*T* conditions are lacking. Let us try to estimate the H-bond lengths in ices at high *P*–*T*. The lengths of hydrogen bonds can be calculated with selected phenomenological model, which describe empirical relation between the H-bond distance O–H…O and the wavenumber of the O–H stretching band, also dealing with distorted two-well potential of H atom.[40–52] We prefer to use simple classic model-1 based on two-well Morse potential[52] for rough estimations of H-bond lengths, namely, O–O separation R_{OO} in H_2O ices using O–H stretching band wavenumbers v_i. According to the relations,[52] successfully applied to H-bond network in thaumasite[32] and parasibirskite,[30] the average H-bond length O–O corresponding to the O–H stretching vibration at 3264 cm^{-1} in ice VII at 3.28 GPa and 22 °C may be estimated as 2.786 Å that is comparable to structural data.[39]

Unusual type of Raman spectrum of modified ice VII with strong abnormal bands marked by asterisks in six and seven plots obtained at the cooling from 373 °C (at 12.5 GPa) to 21 °C (at ~6.6–5.6 GPa) was observed in Fig. 3. The H-bond length (O–O distance) corresponding to the O–H stretching band at 3152 cm^{-1} in this ice VII at 6.62 GPa and 21 °C may be found as 2.736 Å, whereas the O–O distance of H-bond corresponding to the abnormal O–H band at 3260 cm^{-1} may be estimated as 2.784 Å, using the relations.[32,52] Low-wavenumber band at about 315–335 cm^{-1} of this modified ice VII is widened and has several sub-bands in the spectra 7–10 marked 'after cool' in Fig. 2.

We consider that the ice VII′ is formed at 9.8 GPa and 239 °C, exhibiting the strongest Raman O–H band shifted to high wavenumbers up to 3145 cm^{-1} compared with 3111-cm^{-1} band of ice VII at 10.5 GPa and 200 °C (Fig. 3, spectra 13 and 14). The O–O distance of H-bond corresponding to the 3145-cm^{-1} band is estimated as 2.733 Å. The low-wavenumber band of ice VII′ exhibits the shift to lower value 338.3 cm^{-1} and the decrease of bandwidth at 9.8 GPa and 239 °C compared with 345.2-cm^{-1} band of ice VII at 10.5 GPa and 200 °C (Fig. 2, spectra 15 and 16).

There are complex trifurcated H-bonds in muscovite (phengite)[53,54] that need the improvement of model for estimations of R_{OO} distances from O–H stretching bands because available model[32,52] is applicable for calculation of unrolling X–H…Y hydrogen bonds (or for draft estimation of H-bonds with small deviation of angle from 180°).

The position of hydrogen proton H in micas is controlled by an interplay between electrostatic repulsion from M1 and M2 cations on one side of the OH group and a repulsion from extra-sheet cations (K in phengite) and tetrahedral cations on the other side.[9] Using neutron diffraction, Gatta *et al.*[53] determined trifurcated

Table 1. Observed and calculated Raman mode wavenumbers (cm^{-1}) and assignments for phengite-$2M_1$. Lattice-dynamical simulations were performed with LADY software packet[31]

v_i	Exper. (cm^{-1})	Calc. (cm^{-1})	Sym.	Assignment[a]
v_1	84	95	A_g	TO_4 $trans_x$
v_2	97	96	B_g	TO_4 $trans_y$
v_3	191	180	A_g	(O4,O5)$trans_y$ + TO_4 rot_z
v_4	265	260	A_g	(O5,O2,O3,T) $breath_z$ + M–O2 stretch + TO_4 $trans_z$
v_5	316	302	A_g	(O4,O5)$trans_z$ + TO_4 rot_y
v_6	370	363	A_g	(O4)$trans_{x,y}$
v_7	~400	372	A_g	(O4,O5)$trans_y$ + TO_4 rot_x
v_8	423	420	A_g	(O6,O3,O4,O5,T) $breath_z$ + M–O6 stretch + TO_4 $trans_z$ + M2 $trans_y$
v_9	(a)545	530	A_g	M2–O6 stretch + O2–M–O bend (O2)$trans_x$ + M–O1 stretch (minor)
v_{10}	(b)545	537	A_g	M–O1 stretch + M–O6 stretch (minor)
v_{11}	(a)612	605	B_g	M–O stretch: (O6)$trans_z$ + (O1,O2) $trans_{xy}$
v_{12}	(b)612	606	A_g	M–O stretch: (O6)$trans_z$ + (O1,O2) $trans_{xy}$
v_{13}	(a)704	692	A_g	(O3,O4,O5) $breath_z$ + O–T–O bend + T–O–T bend + M2–O2 stretch + (O1↑↑O2)$trans_y$
v_{14}	(b)704	702	A_g	(O3,O4,O5) $breath_z$ + O–T–O bend + T–O–T bend + M2–O2 stretch + (O1↑↓O2)$trans_y$
v_{15}	751	727	A_g	M–O stretch(O6,O1,O2)$trans_{xy}$ + (O1–T–O,O2–T–O)bend
v_{16}	846	810	A_g	M–O stretch(O6,O1,O2)$trans_{xy}$ + (O1–T–O,O2–T–O)bend + (M2)$trans_z$
v_{17}	(a)902	861	A_g	M2–(O6–H) stretch
v_{18}	(b)902	861	B_g	M2–(O6–H) stretch + M–O2 stretch (minor)
v_{19}	1095	1062	A_g	T1–O1 stretch + T2–O2 stretch
v_{20}	1098	1110	A_g	δ(M–O–H) bend
v_{21}	3612	3615	A_g	O–H stretch
v_{22}	3624	3615	B_g	O–H stretch

[a]Designations are following: M = (M1,M2) are octahedral sites; T = (T1,T2) are tetrahedral sites; (a)(b) 545, 612, 704 and 902 are unresolved doublets; stretch, bend, trans and rot are stretching, bending, translational and librational motions, correspondently; (Oi,Oj,Ok) $breath_z$ is the 'breathing' mode with translations of Oi,Oj,Ok oxygen atoms dominantly along *z*, deforming the thickness of octahedral–tetrahedral layer; the underlined denotations show atoms with maximal amplitudes; (O1↑↑O2) $trans_y$ is parallel and (O1↑↓O2) $trans_y$ is antiparallel translations of O1 and O2 along *y*; M2–(O6–H) stretch indicates the joint movement of O6 and H; M–O stretch(O6,O1,O2)$trans_{xy}$ is example of the stretching mode, having the translations of oxygen atoms along *x,y* directions. Calculated very weak Raman modes are not listed.

H-bond in $2M_1$-muscovite: the O6–H bond distance is 0.984 Å at 22 °C, and three significantly weak hydrogen bonds to oxygen atoms, with H···O2 = 2.635, H···O4 = 2.657 and H···O5 = 2.647 Å, and O6–H···O angles all similar value ~138°. Similar configuration of H-bonds is maintained also in $2M_1$- and 3*T*-phengites, using the neutron diffraction data.[54,55] Probably, high thermal stability of phengites in respect to OH^- groups is controlled by such trifurcated H-bonds.

With increase of pressure, no additional bands due to O–H stretching vibrations were observed in the studied mineral, this finding being indicative of the absence of additional water molecules or OH^- groups contained in the extra-sheet space of phengite. Weak variations of the observed Raman O–H band of phengite (from ambient 3612 cm^{-1} to 3580 cm^{-1} at 12.5 GPa, 373 °C) are indicative of high stability of hydroxyls in phengite crystal structure. The absence of additional Raman peaks proves the absence of any non-quenchable phases: no reversible polymorphic transitions, over- or superhydration (previously observed in zeolites[17,18]) or notable amorphization. Following the experiment held at high *P–T* conditions and the subsequent relief of high pressure and temperature, the phengite Raman spectrum reacquires its initial form. In particular, the band due to the O–H vibrations of hydroxyl groups returns to its initial spectral position at 3612 cm^{-1} (Figs 2 and 3).

With increase of *P* at fixed *T* = 22 °C, the dependence of the wavenumber of the 704-cm^{-1} band is linearly increased up to pressure *P* ~ 10 GPa (Fig. 4). Then, the heating of the working volume of DAC was turned on at fixed membrane pressure; this has led to the establishment of nearly isochoric conditions and resulted in a small rise of pressure (Fig. 4). At this stage, the wavenumbers of the bands weakly increased with *T* and *P*, which increase was, first, due to the growth of *P*, whereas the influence of the growth of *T* on the wavenumber normally leads to some reduction of the wavenumber. This *T*-induced reduction only partially compensates for the shift of the wavenumber to higher values caused by the pressure growth.

Initially, the width of the 704-cm^{-1} band weakly increases with the growth of *P* at fixed temperature *T* = 22 °C, this increase being observed up to pressure *P* ~ 10 GPa (Fig. 5). Then, with the heating of the working volume of DAC turned on, this band rapidly widens with the growth of *P* due to the contributions of the two, *T*- and *P*-induced, mechanisms that widen the band during isochoric growth.

According to the data,[1,24–26,56,57] phengite at high *P–T* parameters may transform in another layered mineral that is an analogue of hollandite, $KAlSi_3O_8$. This transformation could be detected by Raman spectrum of K-hollandite: the strongest band at 763 cm^{-1} and strong bands at 217 and 175 cm^{-1} (page 50 in[26]). We did not observe such transformation in our experiments up to maximal parameters *P* ~ 12.5 GPa and *T* ~ 373 °C (Fig. 1), presumably due to very slow kinetics of the transformation at this *T*, a higher stability of our samples resulting from the variation of the chemical content in natural specimens[56] and the degree of structural disorder that is typical for phengites.[57] Moreover, according to available literature data,[24–26,56,57] hollandite synthesis was carried out at temperatures only above 600 °C and experimental *P–T* points are scarce, resulting in unreliable plot of phengite–hollandite transformation for lower temperature.

Conclusions

The performed study of phengite specimens compressed in water medium at 'cold' subduction *P–T* parameters (up to 12.5 GPa and 373 °C) during 4 h has proved stability of the crystal structure of the mineral. This stability was exhibited as the preserved number of registered Raman bands, monotonous evolution of intensities, wavenumbers and widths of the bands, and the absence of new quenchable and non-quenchable phases of the material.

Acknowledgments

This work was supported by the Russian Science Foundation (Grant No. 15-17-30012).

References

[1] M. W. Schmidt, S. Poli, Treatise on geochemistry. in *The Crust* (Ed: R. L. Rudnick), vol. *3*, Elsevier, Oxford, **2003**, pp. 567–591.
[2] N. L. Dobretsov, V. S. Shatsky, R. G. Coleman, V. I. Lennykh, P. M. Valizer, J. G. Liou, R. Zhang, R. J. Beane, *Int. Geol. Rev.* **1996**, *38*, 136.
[3] J. R. Smyth, S. D. Jacobsen, R. J. Swope, R. J. Angel, T. Arlt, K. Domanik, J. R. Holloway, *Eur. J. Mineral.* **2000**, *12*, 955.
[4] M. Rieder, G. Cavazzini, Y. S. D'Yakonov, V. A. Frank-Kamenetskii, G. Gottardi, S. Guggenheim, P. V. Koval, G. Muller, A. M. R. Neiva, E. W. Radoslovich, J. L. Robert, F. P. Sassi, H. Takeda, Z. Weiss, D. R. Wones, *Can. Mineral.* **1998**, *36*, 905.
[5] S. V. Goryainov, A. S. Krylov, A. N. Vtyurin, Y. Pan, *J. Raman Spectrosc.* **2015**, *46*, 177.
[6] G. D. Gatta, P. Lotti, M. Merlini, H.-P. Liermann, A. Lausi, G. Valdrè, A. Pavese, *Phys. Chem. Miner.* **2015**, *42*, 309.
[7] S. V. Rashchenko, A. Y. Likhacheva, S. V. Goryainov, A. S. Krylov, K. D. Litasov, *Am. Mineral.* **2016**, *101*, 431.
[8] G. D. Gatta, M. Merlini, G. Valdrè, H.-P. Liermann, G. Nénert, A. Rothkirch, V. Kahlenberg, A. Pavese, *Phys. Chem. Miner.* **2013**, *40*, 145.
[9] A. C. Rule, S. W. Bailey, *Clay Clay Miner.* **1985**, *33*, 403.
[10] R. Schmid, L. Franz, R. Oberhänsli, S. Dong, *Geol. J.* **2000**, *35*, 185.
[11] R. Coggon, T. J. B. Holland, *J. Metam. Geol.* **2002**, *20*, 683.
[12] P. Comodi, G. D. Gatta, P. F. Zanazzi, D. Levy, W. Crichton, *Phys. Chem. Miner.* **2002**, *29*, 538.
[13] Q. Williams, E. Knittle, H. P. Scott, Z. Liu, *Am. Mineral.* **2012**, *97*, 241.
[14] Q. Liu, Z. M. Jin, J. F. Zhang, *Chin. Sci. Bull.* **2009**, *54*, 2090.
[15] G. D. Gatta, N. Rotiroti, P. Lotti, A. Pavese, N. Curetti, *Phys. Chem. Miner.* **2010**, *37*, 581.
[16] G. D. Gatta, N. Rotiroti, A. Pavese, P. Lotti, N. Curetti, *Z. Kristallogr.* **2009**, *224*, 302.
[17] S. V. Goryainov, R. A. Secco, Y. Huang, A. Y. Likhacheva, *Microporous Mesoporous Mater.* **2013**, *171*, 125.
[18] S. V. Goryainov, A. S. Krylov, A. N. Vtyurin, *Bull. Russ. Acad. Sci. Phys.* **2013**, *77*, 313.
[19] A. Y. Likhacheva, S. V. Goryainov, T. A. Bul'bak, *Am. Mineral.* **2013**, *98*, 181.
[20] A. Y. Likhacheva, S. V. Goryainov, A. S. Krylov, T. A. Bul'bak, P. S. R. Prasad, *J. Raman Spectrosc.* **2012**, *43*, 559.
[21] S. V. Goryainov, A. S. Krylov, A. N. Vtyurin, A. Y. Likhacheva, P. S. R. Prasad, *Bull. Russ. Acad. Sci. Phys.* **2016**, *80*, 522.
[22] F. Datchi, A. Dewaele, P. Loubeyre, R. Letoullec, Y. Le Godec, B. Canny, *High Pressure Res.* **2007**, *27*, 447.
[23] A. S. Krylov, I. A. Gudim, I. Nemtsev, S. N. Krylova, A. V. Shabanov, A. A. Krylov, *J. Raman Spectrosc.* **2017**. DOI: 10.1002/jrs.5078.
[24] M. W. Schmidt, S. Poli, *Earth Planet. Sci. Lett.* **1998**, *163*, 361.
[25] A. Watenphul, B. Wunder, W. Heinrich, *Am. Mineral.* **2009**, *94*, 283.
[26] J. Liu, (Na,K) aluminosilicate hollandites: structures, crystal chemistry, and high-pressure behaviour. Dissertation. Universität Bayreuth, Bayreuth, **2007**.
[27] G. G. Lepezin, A. V. Travin, D. S. Yudin, N. I. Volkova, A. V. Korsakov, *Petrology* **2006**, *14*, 98.
[28] S. V. Goryainov, M. B. Smirnov, *Eur. J. Mineral.* **2001**, *13*, 507.
[29] M. B. Smirnov, A. P. Mirgorodsky, P. Quintard, *J. Mol. Struct.* **1995**, *348*, 159.
[30] S. V. Goryainov, Y. Pan, M. B. Smirnov, W. Sun, J.-X. Mi, *Spectrochim. Acta A* **2017**, *173*, 46.
[31] M. B. Smirnov, V. Yu. Kazimirov, *LADY: software for lattice dynamics simulations, Preprint*, Joint Institute for Nuclear Research, Dubna, **2001**.
[32] S. V. Goryainov, *J. Raman Spectrosc.* **2016**, *47*, 984.
[33] D. A. McKeown, M. I. Bell, E. S. Etz, *Am. Mineral.* **1999**, *84*, 1041.
[34] D. A. McKeown, M. I. Bell, E. S. Etz, *Am. Mineral.* **1999**, *84*, 970.
[35] A. Tlili, D. S. Smith, J.-M. Beny, H. Boyer, *Mineral. Mag.* **1989**, *53*, 165.
[36] P. Pruzan, J. C. Chervin, M. Gauthier, *Europhys. Lett.* **1990**, *13*, 81.
[37] H. Hirai, H. Kadobayashi, T. Matsuoka, Y. Ohishi, Y. Yamamoto, *High Pressure Res.* **2014**, *34*, 289.
[38] M. Somayazulu, J. Shu, C. Zha, A. F. Goncharov, O. Tschauner, H. Mao, R. J. Hemley, *J. Chem. Phys.* **2008**, *128*, 064510
[39] B. Kamb, B. L. Davis, *PNAS* **1964**, *52*, 1433.
[40] N. Rekik, H. Ghalla, N. Issaoui, B. Oujia, M. J. Wojcik, *J. Mol. Struct. (THEOCHEM)* **2007**, *821*, 58.
[41] N. Rekik, F. A. Al-Agel, H. T. Flakus, *Chem. Phys. Lett.* **2016**, *647*, 107.
[42] E. Libowitzky, *Monatsh. Chem.* **1999**, *130*, 1047.
[43] P. Colomban, A. Novak, *J. Mol. Struct.* **1988**, *177*, 277.
[44] P. Colomban, A. Gruger, A. Novak, A. Régis, *J. Mol. Struct.* **1994**, *317*, 261.
[45] N. Rekik, H. Ghalla, H. T. Flakus, M. Jabłońska, B. Oujia, *J. Comput. Chem.* **2010**, *31*, 463.
[46] N. Rekik, H. Ghalla, H. T. Flakus, M. Jabłońska, P. Blaise, B. Oujia, *Chemphyschem* **2009**, *10*, 3021.
[47] N. Rekik, H. T. Flakus, A. Jarczyk-Jędryka, F. A. Al-Agel, M. Daouahi, P. G. Jones, J. Kusz, M. Nowak, *J. Phys. Chem. Solid* **2015**, *77*, 68.
[48] N. Rekik, *Phys. B Condens. Matter* **2014**, *436*, 164.
[49] H. T. Flakus, N. Rekik, A. Jarczyk, *J. Phys. Chem.* **2012**, *A116*, 2117.
[50] H. Ghalla, N. Rekik, A. Michta, B. Oujia, H. T. Flakus, *Spectrochim. Acta* **2010**, *A75*, 37.
[51] M. E. A. Benmalti, A. Krallafa, N. Rekik, M. Belhakem, *Spectrochim. Acta* **2009**, *A74*, 58.
[52] S. V. Goryainov, *Physica B* **2012**, *407*, 4233.
[53] G. D. Gatta, G. J. McIntyre, R. Sassi, N. Rotiroti, A. Pavese, *Am. Mineral.* **2011**, *96*, 34.
[54] A. Pavese, G. Ferraris, V. Pischedda, R. Ibberson, *Eur. J. Mineral.* **1999**, *11*, 309.
[55] A. Pavese, G. Ferraris, M. Prencipe, R. Ibberson, *Eur. J. Mineral.* **1997**, *9*, 1183.
[56] K. J. Domanik, J. R. Holloway, *Lithos* **2000**, *52*, 51.
[57] A. Pavese, V. Diella, *Phys. Chem. Miner.* **2013**, *40*, 375.